

NIH RELAIS Document Delivery

NIH-10286728

JEFFDUYN

NIH -- W1 MA34IF

JOZEF DUYN
10 Center Dirve
Bldg. 10/Rm.1L07
Bethesda, MD 20892-1150

ATTN: SUBMITTED: 2002-08-29 17:22:17
PHONE: 301-594-7305 PRINTED: 2002-09-03 07:25:31
FAX: - REQUEST NO.: NIH-10286728
E-MAIL: SENT VIA: LOAN DOC
7967414

NIH	Fiche to Paper	Journal
TITLE:	MAGNETIC RESONANCE IN MEDICINE : OFFICIAL JOURNAL OF THE SOCIETY OF MAGNETIC RESONANCE IN MEDICINE / SOCIETY OF MAGNETIC RESONANCE IN MEDICINE	
PUBLISHER/PLACE:	Wiley-Liss, Inc., a division of John Wil New York, NY :	
VOLUME/ISSUE/PAGES:	1996 May;35(5):671-7 671-7	
DATE:	1996	
AUTHOR OF ARTICLE:	Liu G; van Gelderen P; Duyn J; Moonen CT	
TITLE OF ARTICLE:	Single-shot diffusion MRI of human brain on a conv	
ISSN:	0740-3194	
OTHER NOS/LETTERS:	Library reports holding volume or year 8505245 8722818	
SOURCE:	PubMed	
CALL NUMBER:	W1 MA34IF	
REQUESTER INFO:	JEFFDUYN	
DELIVERY:	E-mail: jhd@helix.nih.gov	
REPLY:	Mail:	

NOTICE: THIS MATERIAL MAY BE PROTECTED BY COPYRIGHT LAW (TITLE 17, U.S. CODE)

---National-Institutes-of-Health,-Bethesda,-MD-----

Single-Shot Diffusion MRI of Human Brain on a Conventional Clinical Instrument

Guoying Liu, Peter van Gelderen, Jeff Duyn, Chrit T. W. Moonen

A single-shot diffusion MRI technique on a standard clinical 1.5T scanner is presented. The method incorporates the following elements: (a) an inversion RF pulse followed by a delay of 1.3 s to null cerebral spinal fluid (CSF) signal, (b) a stimulated echo sequence ($TE = 56$ ms, $TM = 100$ ms) to obtain strong diffusion weighting, (c) a single-shot gradient- and spin-echo (GRASE) sequence for imaging with a modified k -space trajectory and Carr-Purcell Meiboom-Gill (CPMG)-phase cycle. The trace of the diffusion coefficient obtained with this approach is in good agreement with values reported for animal brain, and for recent human studies. It is demonstrated that single-shot diffusion imaging of human brain is feasible on an unmodified standard instrument without high-gradient slew rate or extreme field homogeneity.

Key words: diffusion; brain; single-shot MRI; gradient and spin echo (GRASE); Carr-Purcell-Meiboom-Gill (CPMG).

INTRODUCTION

NMR has been used to measure the diffusion of liquids since the first years of NMR research (1–5). Recently, MR imaging (MRI) was recognized as an important tool to map noninvasively the diffusion coefficient of water in tissue *in vivo*. Thus, water diffusion was introduced as an additional MRI contrast parameter (6–9). Measurements performed by Moseley *et al.* on cat brain (10, 11) showed that the diffusion coefficient of water is lowered in acute stroke and that diffusion-weighted MRI can be used to detect stroke earlier than conventional MRI techniques. Since then, diffusion MRI has attracted increasing attention in research on animals and in humans (12–21). These studies have convincingly demonstrated that diffusion MRI is a sensitive method for detecting cerebral ischemia at a very early stage, providing physiological information that is not accessible by standard imaging techniques. It has also been shown (17) that images representing the trace of the diffusion coefficient better delineate regions affected by stroke, inasmuch as the trace is independent of orientation effects of myelin fiber.

Despite a number of successful *in vivo* studies on anesthetized animals (10–17), diffusion MRI in the clinical environment requires special attention to motion problems (18–21). Because diffusion experiments are sensitive to micrometer displacements, a small displacement

of the subject during the time interval between the diffusion-sensitizing gradient pulses can create changes in signal phase. In multishot imaging, where data are acquired from multiple excitations, motion-induced signal phase changes can result in significant artifacts and instabilities that interfere with the detection of the diffusion related signal changes. It has been shown that corrections for rigid body motion in multishot diffusion-weighted imaging can be made using navigator echoes (22). Promising results with this technique have been shown recently (23). However, Anderson and Gore (24) have shown that the navigator echo provides sufficient information for such a correction only if the diffusion gradient is applied in the phase-encoding direction. Thus, the use of navigator echoes appears to be of limited value when information about the trace of the diffusion coefficient is needed. In addition, nonrigid body motion cannot be corrected by the navigator echo. These problems can be avoided by using single-shot imaging, where such phase changes do not affect image quality, because the entire k -space is collected with one excitation pulse. Single-shot methods may thus be preferable, despite their lower resolution. Diffusion-weighted echo-planar imaging (EPI) (25, 26) has shown great promise, by demonstrating lesion progression in the penumbra region (21). However, the expensive hardware upgrade and sensitivity to susceptibility effects limit large clinical trials.

In this study, we present a single-shot MRI pulse sequence for the measurement of diffusion on a standard 1.5T clinical instrument. The sequence uses a combination of gradient and spin echoes (GRASE) (27–31) as the single-shot imaging method. Feinberg *et al.* (31) have shown that more echoes, and hence a better resolution, can be obtained with single-shot GRASE imaging than with EPI using the same hardware. However, a standard CPMG cycle cannot be used for the train of refocusing pulses when the GRASE sequence is applied with strong diffusion weighting. Here, we use a modified CPMG phase cycle and k -space trajectory. The sequence was applied to diffusion imaging of human brain on a conventional 1.5T instrument equipped with standard gradients. A preliminary account of this work was presented previously (32).

PULSE SEQUENCE

Diffusion sensitization is commonly achieved by adding a pair of gradient pulses to a standard spin-echo sequence. When strong diffusion sensitivity is desired with relatively weak gradient amplitude and when $T_2 \ll T_1$, it is convenient to use a stimulated echo sequence (3, 5). The pulse sequence for the single-shot diffusion imaging (Fig. 1) consists of three parts: (a) An inversion pulse followed by a delay to null the magnetization of CSF,

MRM 35:671–677 (1996)

From the In Vivo NMR Research Center, BEIP, NCRR (G.L., P.V.G., C.T.W.M.) and the Laboratory of Diagnostic Radiology Research, OIR (J.D.), National Institutes of Health, Bethesda, Maryland.

Address correspondence to: Chrit T. W. Moonen, Ph.D., In Vivo NMR Research Center, BEIP, NCRR, National Institutes of Health, Building 10, Room B1D-125, Bethesda, MD 20892.

Received April 20, 1995; revised October 23, 1995; accepted December 22, 1995.

0740-3194/96 \$3.00

Copyright © 1996 by Williams & Wilkins

All rights of reproduction in any form reserved.

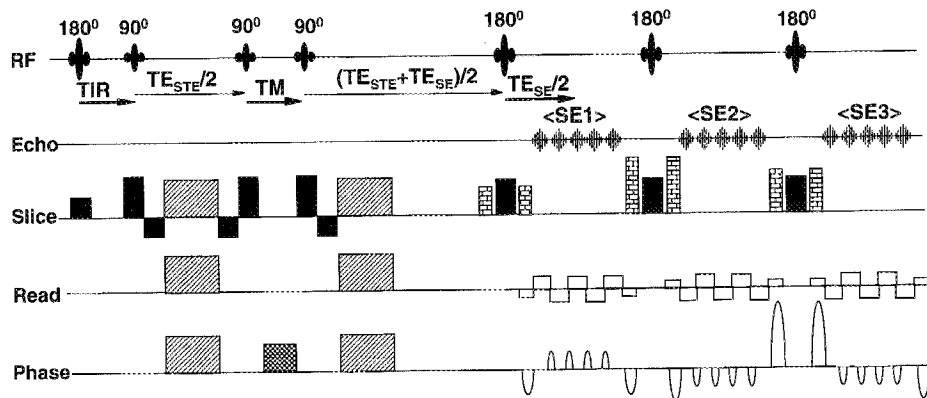


FIG. 1. Pulse sequence for the single-shot diffusion MR imaging comprising: (a) an inversion pulse followed by a delay ($T_I = 1.3$ s) to null the magnetization of CSF, (b) a diffusion-weighted stimulated echo sequence ($TE_{ste}/TM = 56/100$ ms) for diffusion-sensitization, (c) a single-shot acquisition combining gradient and spin echoes (GRASE) for imaging with a time between refocusing RF pulses (TE_{se}) of 20 ms. Note that the time scale for the three elements of the sequence is not identical. The diagram has been shortened to include only three refocusing RF pulses in the GRASE sequence. The actual imaging sequence consisted of nine refocusing RF pulses with five gradient echoes between RF pulses. The length of the train of five gradient echoes was 8.2 ms measured from the start of the first echo to the end of the last echo. Gradient pulses denoted by positive and negative black blocks indicate slice selection gradients and slice-select rephasing gradients, respectively. Gradient pulses denoted by hatched patterns, and brick wall patterns indicate balanced pairs of diffusion gradients and crusher gradients around refocusing RF pulses, respectively. The gradient pulse with checkerboard pattern in the TM period serves to select the stimulated echo. Conventional read-out and phase-encode gradients are similar to those for conventional GRASE imaging, and are indicated without a filling pattern. The fixed crushers around the refocusing pulses along the read axis are not indicated.

(b) a diffusion-weighted stimulated echo sequence ($TE_{ste}/TM = 56/100$ ms) for diffusion sensitization with minimal signal attenuation due to transverse relaxation, and (c) a single-shot GRASE sequence for imaging. The imaging sequence consisted of nine refocusing RF pulses and five gradient echoes between the refocusing pulses. All refocusing pulses were numerically optimized for a flat profile across the slice (33). The method differs from the original GRASE in k -space trajectory and RF phase cycle for refocusing pulses.

K-Space Trajectory

The echoes are phase-encoded according to the k -space trajectory shown in Fig. 2. The five gradient echoes between successive refocusing pulses cover a continuous trajectory (block) of k -space. For optimum signal-to-noise ratio (SNR), k -space is scanned starting from the center. Thus, the five central k -space lines are acquired with the five gradient echoes around the first spin echo (SE1 in Fig. 1). The neighboring block of five k -space lines is acquired with the five gradient echoes of the next spin echo (SE2 in Fig. 1), and so on. In addition, within each block of five gradient echoes, the temporal order of k -space lines is random to avoid a regular T_2^* pattern over k -space. This phase-encoding scheme leads to minimal imaging artifacts caused by the combined T_2 and T_2^* effects. Note that the T_2 (and to a smaller extent T_2^*) decay influences the shape of the point-spread function in GRASE, similar to the influence of T_2^* decay in EPI. See references 27–31 for a thorough discussion.

CPMG Versus Non-CPMG

In a normal spin-echo sequence the starting phase of the transverse magnetization is controlled by RF excitation.

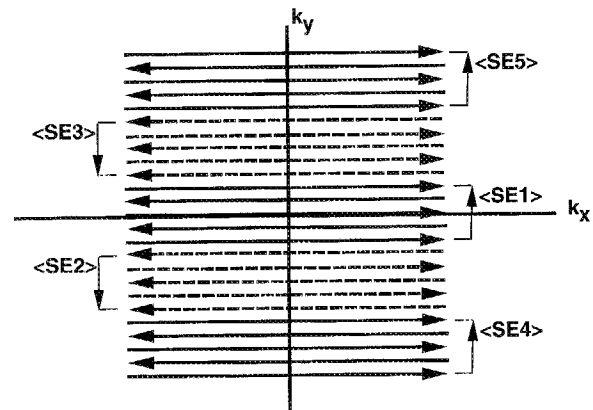


FIG. 2. k -space sampling trajectory for the pulse sequence of Fig. 1. The consecutive numbering of spin echoes in Fig. 1 corresponds with their k -space location as indicated in the figure. The first acquired spin echo, SE1, covers the center of the k -space. Subsequent spin echoes cover an area of k -space progressively extending from the center. The five gradient echoes in each spin-echo period cover a continuous block of k -space. For example, the five central k -space lines are all sampled in the first spin-echo period SE1. During the second spin-echo period, SE2, the five k -space lines indicated by <SE2> are acquired, and so on. However, the order of acquisition of the five k -space lines in each of the nine spin-echo periods is randomized to limit ghosting (31).

In general, a Carr-Purcell Meiboom-Gill (CPMG)-phase cycle is then applied, resulting in substantial cancellation of errors in flip angle. However, when the sequence is strongly sensitized to diffusion, small displacements between the two diffusion-gradient pulses change the phase of the magnetization. As a consequence, the relative phase of the refocusing RF pulse and magnetization is unknown. Thus, the conditions for an effective CPMG

cycle are no longer met. If the phase is 0° or 180° , deviations in the refocusing pulses are compensated (the CPMG effect). If the phase is 90° or 270° , no such effect takes place. The magnetization can thus be viewed as the sum of a CPMG and a non-CPMG component. The unknown relative contribution of the two components has an effect on amplitude and phase of the echoes. The CPMG component decays more slowly than that of the non-CPMG component, depending on the deviations in B_1 field. Because the contribution of the CPMG component is increasing along the spin-echo train, a phase offset is found that changes from echo to echo. A varying amplitude of the sets of crusher gradients around the refocusing pulses can solve these problems. Because the phase of the magnetization at the time of the different RF refocusing pulses will now vary at each point in space, a combination of CPMG and non-CPMG effects will result. So long as the variation in gradient amplitude is sufficient that integration over each voxel will lead to a constant relative contribution of CPMG and non-CPMG effects, a known phase in the echo train is found with respect to the RF pulse. Because the intrinsic CPMG compensation for flip-angle deviations not only takes place between subsequent RF refocusing pulses, but also between pulses further apart in an extended refocusing train, the decay of the signal amplitude resembles more closely a CPMG decay than a non-CPMG decay.

METHODS

A 1.5T GE Signa instrument was used with a standard RF head coil and conventional, shielded gradients with 0.01 Tm^{-1} maximum strength and $17 \text{ Tm}^{-1} \text{ s}^{-1}$ maximum slew rate. The human-subject protocol was approved by the Intramural Review Board at the National Institutes of Health.

Several fine adjustments (tweakers) were implemented in the pulse sequence: (a) dead time twicker placed between onset of read gradient and echo sampling, (b) amplitude tweakers of read-out gradient dephaser and rephaser, (c) amplitude twicker of the slice-selection gradient rephasing lobe, (d) amplitude tweakers of phase-encoding gradients. The first twicker served to eliminate a timing mismatch between the periods of echo sampling and read-out gradient, which was necessary to align the echoes scanned in opposite k_x directions. Further adjustment, which zeroes the first-order phase-fitting parameters for the third gradient echo in each spin echo (zero susceptibility), was done using the second pair of gradient tweakers. The third served to rephase all spins in the slice and maximizes the signal intensity. On our instrument, it was found that the set of gradient tweakers in the phase-encoding direction was not necessary for optimal image quality. The need for such tweakers is probably system dependent.

With nine spin echoes each comprising five gradient echoes, the total number of echoes was 45, with an A/D sampling of 64 data points in 1 ms, leading to a total image time of 170 ms. A 10-mm axial slice was chosen from human brain with an in-plane (nominal) resolution of 3.75 mm (FOV was $240 \times 169 \text{ mm}$). Shimming was performed along the main gradient axes on the slice of

interest. The GRASE image quality is less sensitive to T_2^* effects compared with EPI, because the maximum difference in T_2^* weighting over k -space is reduced in GRASE. Therefore, no extreme shimming efforts were required to produce a reasonable image quality. All RF pulses were applied along the positive x' axis and were made slice selective. The stimulated echo used identical $90^\circ (+x')$ selective-sinc RF pulses. Optimized refocusing pulses (3.2 ms) were utilized for the spin-echo train for an improved (flat) slice profile (33). The slice profile of the refocusing pulses was 10% wider than that of the 90° RF pulses.

To optimally design the sequence for multislice purposes, the preceding inversion pulse was made slice selective. However, because CSF suppression was often found incomplete in the ventricles when using narrow slices (presumably because of flow), a rather thick slice (60 mm) was used here to ensure a high degree of inversion of CSF spins and to limit the influence of CSF flow during the inversion time. The 180° RF pulse that was used for inversion was identical to that used for refocusing pulses. Empirically, an inversion delay of 1.3 s was found to be optimal for CSF suppression.

The varying gradient crushers around each refocusing RF pulse in the GRASE sequence lead to echo amplitudes that are independent of the phase of the starting magnetization, and were arranged as follows: (a) the amplitude of the crusher around the first refocusing pulse is half of that around the second pulse; (b) from the second refocusing pulse on, a progressive decrease in gradient amplitude was used. This particular scheme was used to help avoiding stimulated echoes and creating constant CPMG effects. The degree of attenuation of unwanted stimulated echoes is determined by the dephasing caused by the difference in gradient crushers. The dephasing is most effective along the largest voxel dimension, in this case the slice dimension. Therefore, the varying amplitude crusher was chosen along the slice dimension, similar to an approach used by Crawley and Henkelman (34). The unwanted echoes are predominantly generated along the edges of the slice profile and decrease in amplitude along the train of refocusing pulses (34). This progressive decrease in amplitude of the unwanted echoes led us to double the amplitude of the gradient crushers around the second refocusing pulse, causing a relatively larger attenuation of the first unwanted echo compared with subsequent ones.

A 4-ms gradient crusher along the phase-encoding direction with an amplitude of 7 mTm^{-1} in the TM period (100 ms) was added to select the stimulated echo. A small diffusion weighting ($b = 281 \text{ scm}^{-2}$) was used for the baseline image. For maximum diffusion weighting, gradients of 9.2 mTm^{-1} along all three main axis with $\delta = 20 \text{ ms}$ in both $TE_{\text{str}}/2$ periods were used ($\Delta = 130 \text{ ms}$). Simultaneous gradient pulses along all three principal axes were used to increase the resulting amplitude to 16 mTm^{-1} ($b = 95107 \text{ scm}^{-2}$). For a single slice, five scans were performed with the baseline image followed by four diffusion-weighted images with the relative diffusion-gradient amplitudes of $G_x, G_y, G_z = \{(+1, +1, +1), (+1, -1, +1), (-1, +1, +1), (-1, -1, +1)\}$ and with a repetition time (TR) of 7 s. The experiments were re-

peated up to 4 times for signal averaging. The sum of the diffusion coefficients for the four directions gives the trace of the diffusion coefficient if crossterms with other gradients can be neglected. The pulse sequence of Fig. 1 was designed to yield negligible crossterms with other pulsed gradients (see also Ref. 17). For example, the slice select gradients in the stimulated echo sequence and their refocusing gradient pulses were placed immediately next to each other. With the parameters used in this pulse sequence, the influence of the crossterm with the slice select (z) gradient are calculated to be 0.05% of the main diffusion term (due to the diffusion gradients only). There are no other crossterms with pulsed field gradients. When applied to a sample with strong background (shim) gradients, crossterms with these constant shim gradients may also become a problem (35, 36). However, it can be easily calculated that for the human brain, at 1.5T, such effects can be safely neglected in this new pulse sequence even in the case of relatively poor shimming. For example, a background gradient of 3 Hz per pixel would lead to crossterms of only 0.1% relative to the effect of the applied diffusion gradients. This is insignificant compared with the accuracy in the diffusion maps.

For data processing, the echoes collected with negative read-out gradients were reversed in time. Fourier transformation was applied yielding a 1D profile along the read-out direction. Zero-, first-, and second-order phase correction were applied on the basis of a reference scan without phase-encoding but were otherwise identical to the baseline image. The correction parameters were obtained from a polynomial fit with zero-, first-, and second-order terms of the phase of each Fourier-transformed echo masked with a signal threshold. A separate phase correction was applied for each of the 45 echoes. The phase of the even spin echoes was then flipped with respect to zero. The echoes were reshuffled into their proper position in k -space followed by Fourier transformation along the phase-encode direction. Together with the baseline image, each diffusion-weighted image was used to calculate the diffusion coefficient in the direction of the diffusion gradient for all voxels of the baseline image masked with an intensity threshold of approximately 5 times the standard deviation of the noise. From the sum of the four diffusion coefficients in different directions, the trace of the diffusion image can be obtained.

Cardiac gating effectively improved the quality of the diffusion-weighted images. This was especially evident around the ventricles. The signal intensity in those areas was dependent on the gating delay time (0, 100, 200, 300, 400, 500 ms without inversion pulse, and 0, 100 ms with inversion pulse). All *in vivo* studies were performed with cardiac gating using a TR of 8 cardiac cycles.

RESULTS AND DISCUSSION

In Vitro Studies

The single-shot diffusion method was first applied to a large cylinder (diameter: 14 cm, length: 25 cm) containing doped water with T_2 of 1.1 s to check the accuracy

and reliability of diffusion measurements. Running the GRASE sequence without phase-encoding allowed measurement of the signal attenuation in the spin-echo train and allowed for adjustment of the crusher amplitudes to reach fixed relative contributions of both CPMG and non-CPMG components. We used a combination of a fixed crusher in the x direction with amplitude 6 mTm^{-1} and duration 1.5 ms, and a variable crusher in the z direction with duration 1.5 ms. The progressive attenuation of the amplitude of the z crusher over the spin-echo train was varied until the measured echo decay was independent of the starting phase of the magnetization. Starting with a gradient crusher in the z direction around the second refocusing pulse with amplitude 10 mTm^{-1} , a progressive 10% decrease in amplitude of each subsequent z crusher was found to be sufficient to reach the condition of fixed CPMG and non-CPMG components. Thus, the z crushers around the last refocusing pulse had an amplitude of 3 mTm^{-1} . A decrease of 16% in echo amplitude was found for the last (9th) spin echo. From the T_2 relaxation time, a decrease in echo amplitude of 10% is expected. Therefore, only a 6% further signal attenuation could be attributed to nonideal refocusing pulses. To further evaluate the B_1 homogeneity, the spatial distribution of signal of the last spin echo was compared with that of the first echo showing that 90% of all voxels was within 6% of the average signal drop for the last spin echo. These measurements show that (a) the CPMG effect was independent of starting phase and (b) the B_1 homogeneity of the standard quadrature head coil was sufficient for application to human brain. Fig. 3 shows the baseline image and one of the four diffusion-weighted images, respectively. The four images weighted in the different directions are expected to be identical, due to the isotropic nature of diffusion for water in the phantom. This was confirmed experimentally. Fig. 3 thus shows that the GRASE single-shot diffusion-sensitized pulse sequence can be implemented on a conventional clinical instrument to produce diffusion-weighted images without major artifacts at b values of up to 95, 107 scm^{-2} . SNR was about 220 for the single-shot image. SNR is defined as the average signal divided by the standard deviation of the noise in the read-out direction. SNR decreased to approximately 110 due to 50% signal loss caused by the stimulated echo sequence compared with spin echo. The b -factor of 95,107 scm^{-2} causes approximately a 84% signal attenuation due to diffusion of pure water at 20°C. Therefore, the SNR of the diffusion-weighted single-shot images was approximately 17. The combination of the baseline and four diffusion-weighted images led to a diffusion trace image with SNR of approximately 125 (35), due to signal averaging. Fig. 3 (c) is the map for calculated average diffusion constant D_{av} (one third of the diffusion trace) showing the expected homogeneous diffusion coefficient of water in a large bottle. The histogram of the calculated D_{av} map plotted in Fig. 3 (d) shows a narrow distribution centered around $1.95 \times 10^{-5} \text{ cm}^2 \text{ s}^{-1}$ with standard deviation (SD) of $0.02 \times 10^{-5} \text{ cm}^2 \text{ s}^{-1}$, which is in good agreement with literature values (37) of diffusion constant for bulk water at room temperature. The diffusion measurements from the water phantom show that this sequence gives accu-

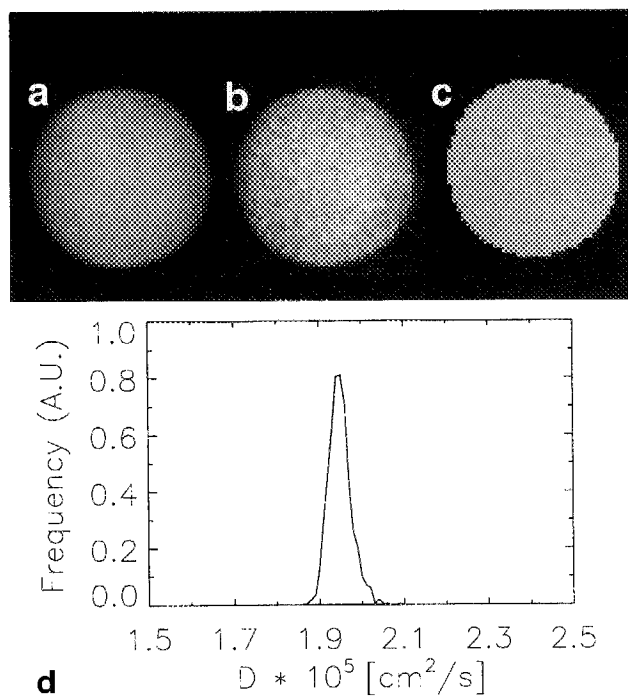


FIG. 3. Images from a diffusion study on a phantom filled with doped water: (a) single-shot baseline image, (b) single diffusion-weighted image ($b = 95107 \text{ scm}^{-2}$) with the diffusion gradients applied along one of the four diagonal directions, (c) the map for calculated average diffusion coefficient D_{av} , or $1/3\text{Tr}(\mathbf{D}')$, (d) the histogram of the calculated D_{av} map with a distribution centered around $1.95 \times 10^{-5} \text{ cm}^2 \text{ s}^{-1}$ (SD: $0.02 \times 10^{-5} \text{ cm}^2 \text{ s}^{-1}$).

rate diffusion coefficients on a conventional whole-body system.

In Vivo Studies

In vivo experiments were done on seven healthy volunteers. All diffusion maps were acquired using identical parameters. An example obtained from a healthy volunteer is shown in Fig. 4. The general quality of baseline image is illustrated in Fig. 4a with contrast similar to those of T_2 -weighted images for a 10-mm axial slice obtained through the ventricles. The phase-encode direction contained some minor intensity artifacts. CSF spaces could be easily identified by their hyperintensity. Fig. 4b represents a single diffusion-weighted image ($b = 95,107 \text{ scm}^{-2}$) with diffusion gradients $G_x, G_y, G_z = (-1, +1, +1)$ along one of the four diagonal directions described in the previous section, whereas Fig. 4c is the average over all four directions. Some intensity variation is found in the single diffusion-weighted image, which could be caused either by the intensity artifacts in the phase-encoding direction or by diffusion anisotropy in the brain. The latter hypothesis was supported by the fact that the intensity variation in the images was found to be strongly dependent on the direction of the diffusion gradient. This effect is greatly reduced in the images weighted with the trace of the diffusion coefficient, in which the orientational dependence is effectively averaged out.

SNR was approximately 130 for the brain tissue in the single-shot baseline image without the diffusion weight-

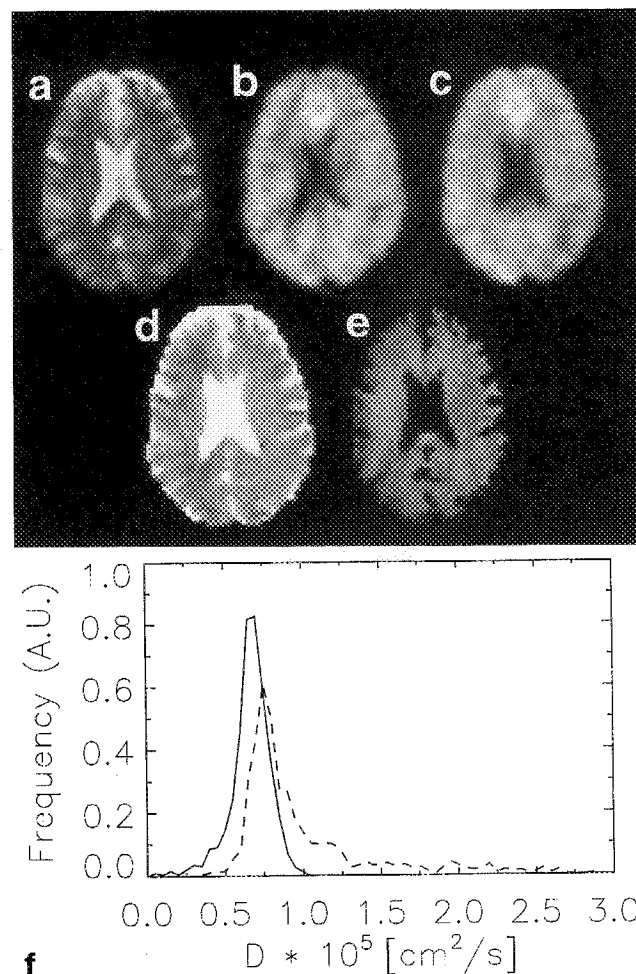


FIG. 4. Axial images through the ventricles from an *in vivo* diffusion study on human brain: (a) single-shot baseline image; (b) single diffusion-weighted image ($b = 95107 \text{ scm}^{-2}$) with the diffusion gradients $G_x, G_y, G_z = (-1, +1, +1)$ applied along one of the four diagonal directions; (c) the average of the four diffusion-weighted images along all four directions; (d) the map for calculated average diffusion coefficient D_{av} , or $1/3\text{Tr}(\mathbf{D}')$ without the use of the inversion-recovery pulse; (e) same as for, d but with the inversion pulse thus excluding the contribution from CSF; (f) the histogram of the calculated D_{av} maps with the inversion pulse (solid curve) and without the inversion pulse (dashed curve).

ing. It decreased to approximately 55 because of signal loss of the stimulated echo sequence as well as the extra periods for both T_2 and T_1 relaxation in brain tissue. The diffusion weighting with a b -factor of $95,107 \text{ scm}^{-2}$ reduces the SNR to 29 due to 47% signal attenuation caused by the diffusion in healthy brain tissue. Thus the combination of the baseline and four diffusion-weighted images plus the four signal averaging led to an average diffusion image with SNR of approximately 68.

Fig. 4d shows the average diffusion map (D_{av}) in the same normal volunteer calculated using the baseline (a) and the diffusion-weighted image (c) as described, without inversion pulse. The D_{av} image clearly showed hyperintensity in the CSF spaces, and an elevated average diffusion constant ($0.97 \times 10^{-5} \text{ cm}^2 \text{ s}^{-1}$), as expected from the known high-diffusion coefficient of water in CSF. The distribution of the diffusion coefficient is de-

picted in Fig. 4f (dashed curve). With the inversion pulse, the signal contribution from CSF is greatly attenuated, and the D_{av} map (Fig. 4e) showed negligible gray/white matter contrast with an average diffusion coefficient of $0.63 \times 10^{-5} \text{ cm}^2 \text{ s}^{-1}$. The histogram (Fig. 4f, solid curve) represents the distribution of diffusion coefficient within the brain tissue. Compared with the experiments without the inversion pulse, the peak is now centered at a lower value of diffusion coefficient and the shoulder representing components with higher diffusion coefficient is removed (no CSF contribution).

Table 1 summarizes the studies on seven normal volunteers with and without the inversion pulse. All studies produced diffusion coefficients in a rather narrow range. The average D compares well with trace(**D**) data of cat brain obtained in this laboratory without CSF nulling (average $D = 0.65 \times 10^{-5} \text{ cm}^2/\text{s}$ in ref. 17). Until now, few data have been reported on trace(**D**) of human and animal brain. Because the diffusion in white matter is highly anisotropic, a comparison for white matter with literature data is not meaningful. Data reported here for gray matter agree well with animal data obtained with diffusion weighting along a single axis (10–17). The average D without CSF nulling compares well with recent data on human brain obtained without CSF nulling (20, 21). Note that the standard deviation of approximately 16% for the diffusion coefficient in human brain after CSF nulling is well below the expected drop of 35%–56% (10–17, 21) in regions affected by acute stroke.

CONCLUSION

A single-shot diffusion imaging method is presented which allows accurate diffusion mapping of human brain on a conventional clinical instrument at 1.5T with gradients of 0.01 Tm^{-1} without any special hardware with a nominal in-plane resolution of 3.75 mm. This study confirms a recent suggestion that GRASE imaging offers potential for single-shot diffusion imaging of human brain (31).

Table 1
Summary of D_{av} (one third of the trace of the diffusion tensor) in seven volunteers with and without inversion pulse

Normal volunteer	D_{av} (in $10^{-5} \text{ cm}^2 \text{ s}^{-1}$) without inversion, average#	D_{av} (in $10^{-5} \text{ cm}^2 \text{ s}^{-1}$) with inversion	
		Average#	SD*
1	1.04	0.65	0.12
2	0.98	0.59	0.13
3	1.01	0.68	0.12
4	1.01	0.62	0.11
5	0.97	0.63	0.11
6	1.03	0.64	0.12
7	0.90	0.56	0.11
Average*	0.99	0.62	0.12

D_{av} values are listed as average with and without the inversion pulse for the CSF nulling. Average# and SD* refer to the average diffusion coefficient D and standard deviation in D for all voxels in one slice with signal intensity above the threshold. Average* in the last row is the average D over all volunteers.

ACKNOWLEDGMENTS

The authors thank Dr. Chris Hardy (GE CR&D) for the optimized refocusing pulses.

REFERENCES

1. E. L. Hahn, Spin echoes. *Phys. Rev.* **80**, 580–594 (1950).
2. H. Y. Carr, E. M. Purcell, Effects of diffusion on free precession in nuclear magnetic resonance experiments. *Phys. Rev.* **94**, 630–638 (1954).
3. D. E. Woessner, NMR spin-echo self-diffusion measurements on fluids undergoing restricted diffusion. *J. Phys. Chem.* **67**, 1365–1367 (1963).
4. E. O. Stejskal, J. E. Tanner, Spin diffusion measurements: Spin echoes in the presence of a time-dependent field gradient. *J. Chem. Phys.* **42**, 288–292 (1965).
5. J. E. Tanner, Use of the stimulated echo in NMR diffusion studies. *J. Chem. Phys.* **52**, 2523–2526 (1970).
6. G. E. Wesbey, M. E. Moseley, R. L. Ehman, Translational molecular self-diffusion in MRI measurements of the self-diffusion coefficient. *Invest. Radiol.* **19**, 491–498 (1984).
7. D. G. Taylor, M. C. Bushell, The spatial mapping of translational diffusion coefficients by the NMR imaging technique. *Phys. Med. Biol.* **30**, 345–349 (1985).
8. K. D. Merboldt, W. Hänicke, J. Frahm, Self diffusion NMR imaging using stimulated echoes. *J. Magn. Reson.* **64**, 479–486 (1985).
9. D. Le Bihan, E. Breton, D. Lallemand, P. Grenier, E. Gabanis, M. Laval-Jeantet, MR imaging of intravoxel incoherent motion: Application to diffusion and perfusion in neurologic disorders. *Radiology* **161**, 401–407 (1986).
10. M. E. Moseley, Y. Cohen, J. Mintorovitch, J. Kucharczyk, P. R. Weinstein, Early detection of regional cerebral ischemia in cats: Comparison of diffusion- and T_2 -weighted MRI and spectroscopy. *Magn. Reson. Med.* **14**, 330–346 (1990).
11. M. E. Moseley, Y. Cohen, J. Kucharczyk, J. Mintorovitch, H. S. Asgari, M. F. Wendland, J. Tsuruda, D. Norman, Diffusion-weighted MR imaging of anisotropic water diffusion in cat central nervous system. *Radiology* **176**, 439–445 (1990).
12. A. L. Busza, K. L. Allen, M. D. King, N. van Bruggen, S. R. Williams, D. C. Gadian, Diffusion-weighted imaging studies of cerebral ischemia in gerbils: Potential relevance to energy failure. *Stroke* **23**, 1602–1612 (1992).
13. R. A. Knight, R. J. Ordidge, J. A. Helpert, M. Chopp, L. C. Rodolosi, D. Peck, Temporal evolution of ischemic damage in rat brain measured by proton nuclear magnetic resonance imaging. *Stroke* **22**, 802–808 (1991).
14. H. Benveniste, L. W. Hedlund, G. A. Johnson, Mechanism of detection of acute cerebral ischemia in rats by diffusion-weighted magnetic resonance microscopy. *Stroke* **23**, 746–754 (1992).
15. B. J. Dardzinski, C. H. Sotak, M. Fisher, Y. Hasegawa, L. Li, K. Minematsu, Apparent diffusion coefficient mapping of experimental focal cerebral ischemia using diffusion-weighted echo-planar imaging. *Magn. Reson. Med.* **30**, 318–325 (1993).
16. M. Takahashi, B. Fritz-Zieroth, T. Chikugo, H. Ogawa, Differentiation of chronic lesions after stroke in stroke-prone spontaneously hypertensive rats using diffusion weighted MRI. *Magn. Reson. Med.* **30**, 485–488 (1993).
17. P. van Gelderen, M. H. M. de Vleeschouwer, D. DesPres, J. Pekar, P. C. M. van Zijl, C. T. W. Moonen, Water diffusion and acute stroke. *Magn. Reson. Med.* **31**, 154–163 (1994).
18. T. L. Chenevert, J. A. Brunberg, J. Pipe, Anisotropic diffusion in human white matter: Demonstration with MR techniques in vivo. *Radiology* **177**, 401–405 (1990).
19. S. Warach, D. Chien, W. Li, M. Ronthal, R. R. Edelman, Fast

- magnetic resonance diffusion-weighted imaging of acute human stroke. *Neurology* **42**, 1717-1723 (1992).
20. D. Chien, K. K. Kwong, D. R. Gress, F. S. Buonanno, R. B. Buxton, B. R. Rosen, MR diffusion imaging of cerebral infarction in humans. *Am. J. Neuroradiol.* **13**, 1097-1102 (1992).
 21. S. Warach, J. Gaa, B. Siewert, P. Wielopolski, R. R. Edelman, Acute human stroke studied by whole brain echo planar diffusion-weighted magnetic resonance imaging. *Ann Neurol.* **37**, 231-241 (1995).
 22. R. J. Ordidge, J. A. Helpem, Z. X. Qing, R. A. Knight, V. Nagesh, Correction of motional artifacts in diffusion-weighted MR images using navigator echoes. *Magn. Reson. Imaging* **12**, 455-460 (1994).
 23. A. de Crespigny, M. Marks, D. Enzmann, M. Moseley, Navigated diffusion imaging of normal and ischemic human brain. *Magn. Reson. Med.* **33**, 720-728 (1995).
 24. A. W. Anderson, J. C. Gore, Analysis and correction of motion artifacts in diffusion weighted imaging. *Magn. Reson. Med.* **32**, 379-387 (1994).
 25. H. E. Avram, L. E. Crooks, Effect of self-diffusion on Echo Planar Imaging, in "Proc., SMRM, Seventh Annual Meeting, 1988," p. 980.
 26. R. Turner, D. Le Bihan, J. Maier, R. Vavrek, L. K. Hedges, J. Pekar, Echo-planar imaging of intravoxel incoherent motions. *Radiology* **177**, 407-414 (1990).
 27. K. Oshio, D. A. Feinberg, GRASE (gradient- and spin-echo) imaging: A novel fast MRI technique. *Magn. Reson. Med.* **20**, 344-349 (1991).
 28. D. A. Feinberg, K. Oshio, GRASE (gradient- and spin-echo) MR imaging: A new fast clinical technique. *Radiology* **181**, 597-602 (1991).
 29. D. A. Feinberg, K. Oshio, Gradient-echo shifting in fast MRI techniques (GRASE imaging) for correction of field inhomogeneity errors and chemical shift. *J. Magn. Reson.* **97**, 177-183 (1992).
 30. K. Oshio, D. A. Feinberg, Single-shot GRASE imaging without fast gradients. *Magn. Reson. Med.* **26**, 355-360 (1992).
 31. D. A. Feinberg, B. Kiefer, G. Johnson, GRASE improves spatial resolution in single shot imaging. *Magn. Reson. Med.* **33**, 529-533 (1995).
 32. C. Liu, P. van Gelderen, C. T. W. Moonen, Single-shot diffusion MRI on a conventional clinical instrument, in "Proc. SMR, 2nd Annual Meeting, 1994," p. 1034.
 33. M. O'Donnell, W. J. Adams, Selective time-reversal pulses for NMR imaging. *Magn. Reson. Imaging* **3**, 377-382 (1985).
 34. A. P. Crawley, R. M. Henkelman, Errors in T_2 estimation using multislice multiple-echo imaging. *Magn. Reson. Med.* **4**, 34-47 (1987).
 35. P. van Gelderen, Diffusion techniques for *in vivo* NMR, Ph.D. thesis, *Delft University Press, Delft, The Netherlands*, (1993).
 36. S. Mori, P. C. M. van Zijl, Diffusion weighting by the trace of the diffusion tensor within a single scan. *Magn. Reson. Med.* **33**, 41-52 (1995).
 37. R. Mills, Self-diffusion in normal and heavy water in the range 1-45°. *J. Phys. Chem.* **77**, 685-688 (1973).